Mechanisms for *p*-type behavior of ZnO, $Zn_{1-x}Mg_xO$, and related oxide semiconductors

Daniel F. Urban,[1,*] Wolfgang Körner,[1,†] and Christian Elsässer[1,2]

[1]*Fraunhofer Institute for Mechanics of Materials IWM, Wöhlerstrasse 11, 79108 Freiburg, Germany*

[2]*Freiburg Materials Research Center, University of Freiburg, Stefan-Meier-Strasse 21, 79104 Freiburg, Germany*

(Received 26 February 2016; revised manuscript received 25 July 2016; published 18 August 2016)

The possibilities of turning intrinsically *n*-type oxide semiconductors like ZnO and $Zn_{1-x}Mg_xO$ into *p*-type materials are investigated. Motivated by recent experiments on $Zn_{1-x}Mg_xO$ doped with nitrogen, we analyze the electronic defect levels of point defects N_O, v_{Zn}, and N_O-v_{Zn} pairs in ZnO and $Zn_{1-x}Mg_xO$ by means of self-interaction-corrected density functional theory calculations. We show how the interplay of defects can lead to shallow acceptor defect levels, although the levels of individual point defects N_O are too deep in the band gap to be responsible for *p*-type conduction. We relate our results to *p*-type conduction paths at grain boundaries seen in polycrystalline ZnO and develop an understanding of a *p*-type mechanism which is common to ZnO, $Zn_{1-x}Mg_xO$, and related materials.

DOI: 10.1103/PhysRevB.94.075140

I. INTRODUCTION

Zinc oxide is a prominent example of an intrinsically *n*-type semiconductor. Its abundant availability, its low-cost production, and its wide electronic band gap of approximately 3.4 eV make ZnO attractive for transparent and conducting oxide layers in consumer-electronics devices. However, a breakthrough of ZnO-based transparent electronics has not been achieved so far due to the lack of sufficiently conductive and long-term stable *p*-type ZnO layers. The problem of *p*-type doping of ZnO has now been a scientific challenge for more than two decades. Besides doping with single elements like N, P, As, or Sb substituting O and Li, Na, K, Cu, Ag, or Au substituting Zn [1–6], codoping was discussed as well [7–9]. Apparently, the most promising candidate so far is still nitrogen. However, it was shown theoretically [10–12] that the substitutional defect of N on O sites (N_O) cannot be responsible for the *p*-type conduction which has been observed in some experiments [13] since it creates a defect level which is located too high above the valence-band (VB) edge with respect to thermal excitation energies.

Recent theoretical and experimental studies consider more complicated defect complexes which involve zinc vacancies (v_{Zn}) or codoping, like the N_O-v_{Zn} and N_O-v_{Zn}-H defect complexes, as potential sources of *p*-type conduction [14,15].

For polycrystalline ZnO it has been proposed that conduction channels of *p* type can be found along grain boundaries [12,16]. Here it is an interplay of grain boundaries, their depletion regions, and point defects that results in the desired low-lying acceptor levels.

It has been reported by Hierro *et al.* [17] that the use of ternary ZnO-based alloys like $Zn_{1-x}Mg_xO$ (denoted by ZMO in the following) facilitates the *p*-type conductivity due to lower net electron concentrations than in pure ZnO. These authors relate the reduced net electron concentration to two deep-lying Mg-related defects which act as electron traps. ZMO retains the wurtzite crystal structure of ZnO for Mg substituting Zn for concentrations up to $x \approx 40\%$, and also the lattice parameters change only slightly. Hence combining ZMO with *n*-type ZnO layers leads to negligible lattice misfits [17].

Up to now it is not yet clear which atomic or extended defects provide the key to promote *p*-type conductivity in ZnO and related materials like ZMO. An understanding of this defect physics would allow targeted development of experimental routes to synthesize materials with these particular acceptor states.

In this paper we present a density functional theory (DFT) study determining the electronic defect levels of the defects N_O, v_{Zn}, and N_O-v_{Zn} in ZnO and ZMO. We discuss our results in the context of the accumulated experimental and theoretical knowledge, and thereby we shed light on the question of why some experimental routes recently taken have led to *p* conduction but others have not. Are the defect states that originate from N_O indeed too deep [10,12] in the band gap? What changes when N_O forms a defect complex with a Zn vacancy, and how do Mg atoms nearby affect its defect level position? To determine the electronic defect levels we use a self-interaction-corrected (SIC) local-density approximation (LDA) approach [12] that is capable of giving far better results than both commonly used approximations, the LDA and the generalized gradient approximation (GGA). The latter two have limited predictive power for wide-band-gap semiconductors due to their inherent significant underestimation of the band gap due to their self-interaction error. SIC-LDA overcomes this limitation and yields electronic band structures with band gaps that are in good agreement with experiment [12,18] and in particular for ZnO a correct separation of the Zn 3*d* and O 2*p* bands [19]. By means of this approach, the defect levels in various amorphous oxide semiconductors based on In, Sn, and Zn have been predicted reliably [20–23].

The results presented in this paper may solve the controversial problem that individual N_O defects are indeed creating levels lying too deep inside the band gap even though nitrogen doping has been observed to lead to *p*-type ZnO and ZMO, probably due to an interplay with other defects. Moreover, we relate our present results to the *p*-type conduction effects which have been observed for grain boundaries in ZnO, and we relate all this to one common origin. The emerging

*daniel.urban@iwm.fraunhofer.de

†wolfgang.koerner@iwm.fraunhofer.de

theoretical picture will presumably be useful for the experimental optimization of p-type conduction in ZnO and ZMO.

II. COMPUTATIONAL APPROACH

A. Supercell models

For the study of defect complexes we have chosen a supercell model of the wurtzite crystal structure of ZnO containing 72 atoms and consisting of $3 \times 3 \times 2$ primitive unit cells. Since $Zn_{1-x}Mg_xO$ retains the wurtzite structure for Mg concentrations $x \leqslant 40\%$ [17]. the corresponding supercells were generated by randomly substituting Zn atoms with Mg atoms. For the study of the bulk crystal properties like lattice parameters and band gap as a function of the Mg concentration we compared several realizations of random Mg distributions within the 72-atom supercell, and we found a negligible dependency of these properties on the Mg distribution. For comparison, we also examined results from a 36-atom supercell in the study of bulk properties. For the subsequent study of defects we have chosen the specific Mg concentration of $x = 1/9 \sim 11\%$ (i.e., replacing 4 of 36 Zn atoms with Mg atoms in the 72-atom supercell), which is representative of typical experimental concentrations [24]. Furthermore, the defect analysis concentrates on specific realizations of the Mg distribution which differ in the number of Mg atoms that cluster in the direct neighborhood of the N_O point defect under study. Two such realizations are displayed in Fig. 1.

B. Structure optimization

The structure optimization of all the constructed supercell models was carried out using the projector augmented-wave (PAW) method [25] as implemented in the VASP code [26,27]. The LDA was used for the exchange-correlation functional, and PAW potentials were used to describe Zn $(3d,4s,4p)$, Mg $3s$, and O $(2s,2p)$ as valence electrons. All VASP calculations were carried out with a plane-wave cutoff energy of 400 eV, a $3 \times 3 \times 3$ Monkhorst-Pack k mesh, and a Gaussian broadening of 0.1 eV.

For all bulk structures the volume optimization was carried out by fitting the universal equation of state [28] to a data set of minimal total energies calculated at different cell volumes. Optimization of the lattice parameter ratio c/a and internal relaxation of the atomic positions were achieved by minimizing the elastic stress and the forces acting on the atoms,

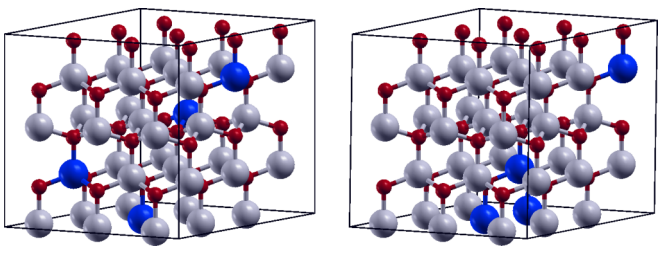

FIG. 1. Two examples of supercell models $Zn_{32}Mg_4O_{36}$ with randomly distributed Mg atoms (left) and with clustered Mg atoms (right). Large gray and blue spheres represent Zn and Mg atoms, respectively. Small red spheres represent oxygen atoms.

respectively. The supercells containing defects were internally relaxed at fixed volume and c/a ratio.

C. Electronic-structure calculations

The electronic-structure calculations on the basis of the SIC-LDA were performed using the computational mixed-basis pseudopotential (MBPP) method [29–32] with the same calculation setup as reported in previous papers [12,33,34]. We have taken the LDA for exchange correlation as parametrized by Perdew and Zunger [35]. For Zn, Mg, and O optimally smooth norm-conserving pseudopotentials [36] were constructed, and a mixed basis of plane waves and nonoverlapping localized orbitals were used. Due to the localized orbitals a plane-wave cutoff energy of 20 Ry (1 Ry = 13.606 eV) is sufficient to obtain well-converged results. For the k-point sampling of the Brillouin-zone integrals a Monkhorst-Pack mesh of $3 \times 3 \times 3$ and a Gaussian broadening of 0.2 eV were used. The densities of states of the supercells were evaluated with the same mesh and a Gaussian broadening of 0.1 eV.

The self-interaction of the LDA is corrected by an incorporation of the SIC in the pseudopotentials [12,37]. The SIC procedure uses weight factors $w = (w_s,w_p,w_d)$ accounting for the occupations of the individual s, p, and d valence orbitals. We corrected the Zn $3d$ semicore orbitals by 100%, i.e., $\boldsymbol{w}_{Zn} = (0,0,1)$. The localized O $2s$ semicore orbitals are also corrected by 100%, while for the spatially more extended O $2p$ valence-band orbitals we have taken 80%, which implies the weight factors $\boldsymbol{w}_O = (1,0.8,0)$. We did not apply a SIC to the almost unoccupied Mg $3s$ and $3p$ and Zn $4s$ and $4p$ conduction-band orbitals of the almost fully ionic compounds $Zn_{1-x}Mg_xO$. For the adjustment of the atomic SIC to the crystal field in the solids, a scaling factor $\alpha = 0.8$ is applied.

III. RESULTS AND DISCUSSION

A. Lattice parameters

The functional dependencies of the lattice parameters a and c on the Mg content are displayed in Fig. 2. Our results underestimate the experimental values by about 1%, which is a typical systematic deviation for LDA results. The increase of a and the decrease of c with increasing Mg content are quantitatively correct and just slightly shifted with respect to previous experimental [38–42] and theoretical [43] findings. This good agreement on the structural parameters is the prerequisite for the electronic structure calculations which are the focus of this work. Note that the deviations from Vegard's rule in some of the values of the experimentally observed lattice constants is probably related to the quality of the thin films and maybe due to the presence of compensated defects or residual strain as discussed, e.g., by Ryoken *et al.* [38].

B. Band gap of ZMO

Theoretical and experimental values of the band gap of $Zn_{1-x}Mg_xO$ as a function of the Mg content x are displayed and compared in Fig. 3. The results obtained with the SIC-LDA approach not only show the rising trend correctly but also show that the calculated values agree quantitatively well with the experimental data. The dependency of the band gap on the

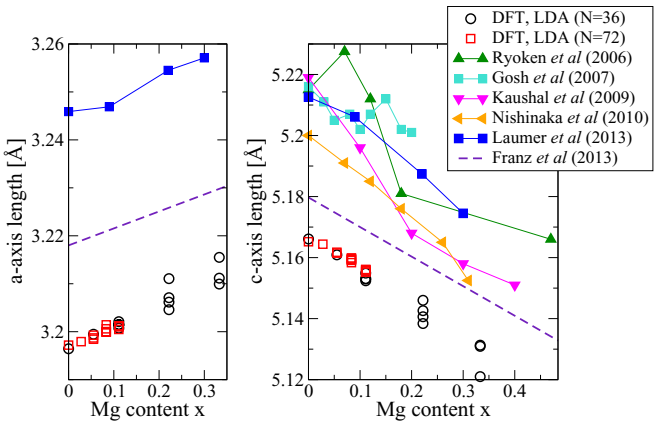

FIG. 2. Lattice parameters obtained by DFT structure optimization of ZMO supercells with $N = 36$ (open circles) and $N = 72$ (open squares) atoms as a function of the Mg content in comparison to experimental data [38–42] (solid symbols) and the result of a recent DFT study [43] (dashed line), taken from the literature. Experimental data points are connected by straight solid lines to guide the eyes.

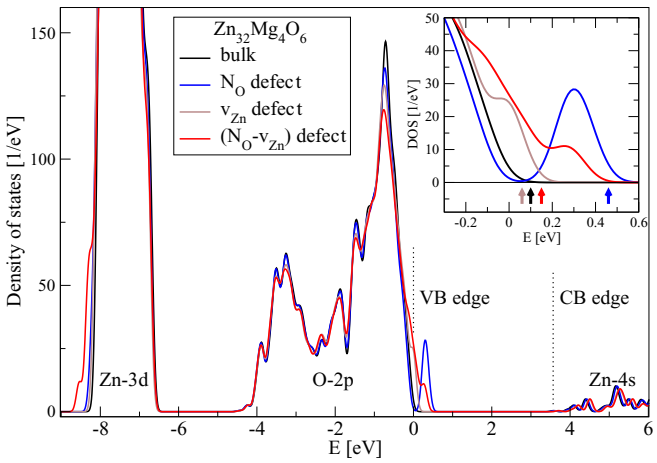

FIG. 4. Comparison of the total DOS of $Zn_{32}Mg_4O_{36}$ without (bulk) and with N_O, v_{Zn}, and N_O-v_{Zn} defects. The inset magnifies the region close to the VB maximum. Small colored arrows on the energy axis mark the highest occupied levels. The curves are aligned with respect to the valence band, and the energy of the bulk VB edge is set to zero.

specific distribution of Mg atoms within the supercell is small; for example, for the sample structures with $x \sim 22\%$ we find an energy scatter of only $\delta E \sim 10$ meV.

The wide scatter of experimental results in Fig. 3 is probably due to the varying quality of the thin films but also due to different experimental approaches of determining the band gaps [38,39,44–46]. Above the thermodynamical solubility limit of $x \sim 5\%$ a nonequilibrium solid solution is formed. Depending on the route of synthesis, this results in compositional nonuniformity, which then leads to the generation of nonequilibrium compensated defects [39] or even structural inhomogeneity [38] and residual elastic stress. Naturally, all of this is reflected in the measured physical properties of the films, as discussed in the respective articles.

For our investigation the calculation of the band gap as a function of the Mg content serves as a validation that the SIC-LDA describes the electronic structure of the Zn-Mg-O system rather well.

The total density of states (DOS) of a representative $Zn_{32}Mg_4O_{36}$ sample calculated with the SIC-LDA approach is shown in Fig. 4. The upper part of the VB is mainly formed by the O $2p$ valence orbitals, while the lower part is dominated by the Zn $3d$ semicore orbitals. Experimentally, the average d-band energy of ZnO was determined to be -7.8 eV relative to the VB edge [47]. This is almost unchanged when Mg is introduced. The SIC-LDA approach reproduces this experimental observation, in contrast to LDA, GGA, and several commonly used hybrid functionals which place the Zn $3d$ levels too high in energy and therefore overestimate their hybridization with the O $2p$ levels. The latter can lead to the wrong positions of defect levels in the band gap [19]. Thus these results validate our approach to analyze individual electronic levels of point defects using the SIC-LDA approach.

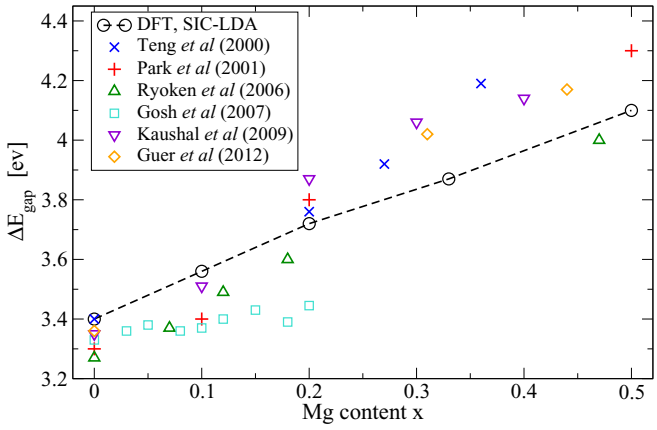

FIG. 3. Band gap of $Zn_{1-x}Mg_xO$ as a function of the Mg content x. The data points calculated with SIC-LDA are connected by a black dashed line to guide the eyes. Experimental data from several groups are shown for comparison [38,39,44–46].

C. Electronic defect levels near the VB

From the total DOS in Fig. 4 it can be seen that the defects N_O, v_{Zn}, and N_O-v_{Zn} create energy levels close to the VB edge. However, a closer inspection, which is provided in the inset, shows that the defect levels that originate from N_O are separated from the VB with a peak at about 0.25 eV. In the left panel of Fig. 5 the position of the N_O defect level is shown as a function of the number of nearest Mg neighbors (NN). Here NN-1Mg indicates a $Zn_{32}Mg_4O_{35}N$ (or $Zn_{31}Mg_4O_{35}N$) supercell in which one Mg atom is adjacent to the N_O (or N_O-v_{Zn}) defect, while in the NN-2Mg and NN-3Mg supercells, two and three Mg atoms are nearest neighbors of the defect.

An increasing number of NN Mg atoms leads to an upshift of the defect level. Therefore, concerning p-type conductivity, Mg doping makes N_O defects less attractive since the level becomes more narrow and moves deeper into the band gap. On the other hand, the energy level position of the N_O-v_{Zn} defect

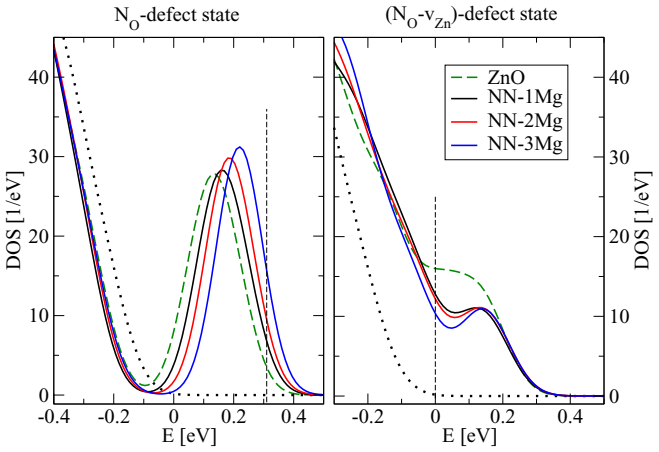

FIG. 5. Section of the total DOS in the vicinity of the VB edge of $Zn_{32}Mg_4O_{36}$ doped with N_O (left) and $N_O + v_{Zn}$ (right), calculated with the SIC-LDA, as a function of the number of nearest-neighbor Mg atoms. For comparison, results for defects in ZnO are shown as dashed lines, and the DOS of perfect ZnO is included as a dotted line.

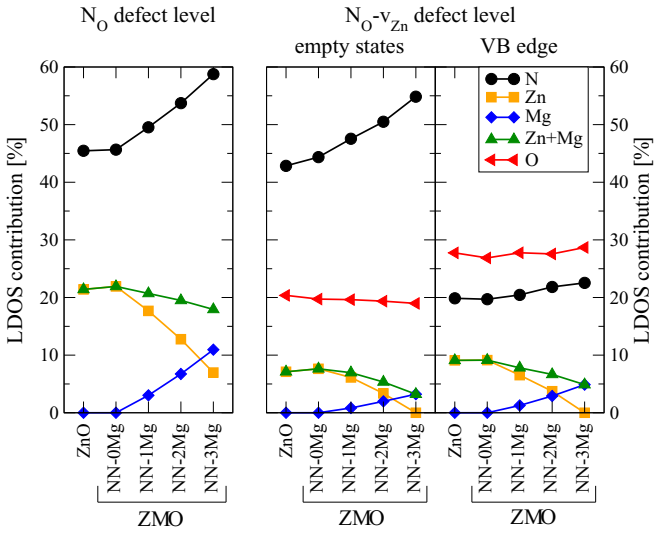

FIG. 6. Relative LDOS contributions to the total DOS of the N_O-defect level (left), the unoccupied part of the $(N_O\text{-}v_{Zn})$-defect level (middle), and the respective VB edge (right), shown for the N_O atom and its most relevant neighbors. The relative positions of these atoms, which are the ones most involved in the defect complex, are sketched on the left in Fig. 7. For the oxygen and metal ions the summed contributions are shown.

complex remains almost unchanged for different numbers of NN Mg atoms.

The substitution of Zn by Mg in ZnO does not help to make the acceptor levels of individual N_O defects shallow, which would facilitate *p*-type conductivity at room temperature, but rather provokes the contrary. Moreover, it has been reported [48] that the presence of Mg atoms in the neighborhood of a N_O defect increases the defect formation energy considerably and therefore reduces the respective defect concentration in the material. Our calculations are in line with the findings of Ref. [48] (see discussion in the Appendix).

Zinc vacancy defects alone create very shallow defect levels (see inset of Fig. 4), which is a well-known result from previous studies [33]. Experimentally, defect levels at either 130 meV [13], 160 meV [24], or 190 meV [49] have been reported, depending on the specific experiment. According to Fig. 5, the levels of the $N_O\text{-}v_{Zn}$ defect complex lie higher above the VB edge than that of the individual v_{Zn} defect and fit the experimentally determined values rather well. We thus propose to assign the experimentally found acceptor levels to a $N_O\text{-}v_{Zn}$ defect complex. This complex is very promising since it provides shallow defect levels that are not separated in energy from the VB edge, and thus continuous low-energy excitation are possible. The position of the defect level varies only slightly with the number of Mg atoms near the defect complex (see right panel of Fig. 5).

D. Spatial distribution of N_O and $N_O\text{-}v_{Zn}$ defect levels

In order to analyze the spatial distribution of the defect levels we have evaluated the atom-projected local densities of states (LDOS) for the most relevant atoms involved in the defect (complex). Figure 6 displays their contributions to the defect levels, while the relative locations of these atoms are sketched in Fig. 7(a). The contribution of an individual neighbor atom to a defect level is evaluated by integrating the LDOS of the respective atom in the relevant energy interval and subsequent division by the sum of the LDOS of all atoms in the supercell, integrated for the same energy range. The energy interval $[-0.1, 0.5]$ eV was chosen for the analysis of the N_O defect, while the analysis of the $N_O\text{-}v_{Zn}$ defect complex is carried out separately for the intervals $[-0.2, 0.0]$ eV (VB edge) and $[0.0, 0.4]$ eV (unoccupied states above the VB edge; see Fig. 5).

Note that the contributions of the oxygen ions (red line) and metal ions (green line) shown in Fig. 6 are the sums of the three O atoms [numbered 1–3 in Fig. 7(a)] and the three or four metal atoms [numbered 4–7 in Fig. 7(a)], respectively.

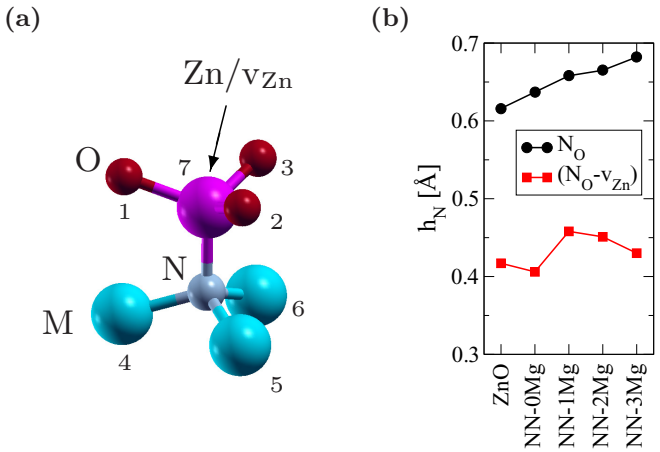

FIG. 7. (a) Sketch of the most relevant atoms involved in the defects N_O and $N_O + v_{Zn}$. Metal atoms on positions 4–6 can be either Zn or Mg. Position 7 corresponds to either a Zn atom or a Zn vacancy. (b) Dependency of the N atom position (height h_N) above the atomic plane defined by the metal atoms 4–6 on the number of Mg atoms involved.

The metal atoms at positions 4–6 can be either Zn or Mg, while position 7 corresponds to either a Zn atom in the case of the N_O defect or a Zn vacancy in the case of the N_O-v_{Zn} defect complex.

The N_O defect level is highly localized on the central N atom by more than 45%, as can be seen from the left panel in Fig. 6. About 20% is shared by the four NN metal atoms, while the oxygen atoms of the second-nearest-neighbor shell contribute 2% or less each. The localization on the N atom increases to ∼60% with an increasing number of NN Mg atoms, while the total contribution of the NN metal atoms remains rather constant. This increase in localization is connected to an increasing spatial separation of the N atom from the plane defined by the three metal atoms labeled 4–6 with an increasing number of Mg atoms therein [see graph in Fig. 7(b)].

The analysis of the spatial distribution of the N_O-v_{Zn} defect (see the middle and right panels in Fig. 6) is divided into two parts, namely (i) the unoccupied states above the VB edge and (ii) the VB edge which is modified with respect to the bulk material by the presence of the defect. The unoccupied states (middle panel in Fig. 6) are reminiscent of the N_O defect, and the N atom contributes more than 40% in pure ZnO, which increases up to 55% with an increasing number of NN Mg atoms. The hybridization with the v_{Zn} defect state results in a 20% contribution of the three oxygen atoms next to the vacancy site. The three remaining NN metal atoms [numbered 4–6 in Fig. 7(a)] only contribute ≈ 2%–3% (Zn) and ≈ 1% (Mg) each. For the VB edge (right panel in Fig. 6), reminiscent of the v_{Zn} defect, the three oxygen atoms are more important (≈ 27%), but the N atom still contributes, on average, ≈ 20%. A change in the number of NN Mg atoms has only a small effect on this spatial distribution with a small shift of weight from the NN metal atoms to N.

E. Defect-complex mechanism for the p-type conduction mechanism

For p-type conduction a Fermi level close the VB edge and shallow acceptor levels in sufficiently high concentration are needed. Since the thermal excitation energy at room temperature is only about 25 meV, p-type conduction with a significant hole concentration can, at best, be achieved by acceptor defect levels which are distributed continuously right above the VB edge. Our SIC-LDA analysis of the most relevant defects in N-doped ZMO shows that v_{Zn} and N_O-v_{Zn} indeed provide such defect levels.

Our results support the hypothesis that codoping of ZnO with Mg and N can be a possible route to obtain p-type conductivity. The N_O-v_{Zn} defect complex yields shallow acceptor levels which can be activated by the experimentally reported lowering of the net electron concentration in ZMO [17,50,51]. This carrier compensation effect increases linearly with the Mg content and can be explained by deep-lying Mg-related defects which act as charge traps [17].

Zinc vacancies are low-lying energy defects which exist also in pure ZnO [33]. However, pure ZnO usually is an intrinsically n-type semiconductor since donor defects dominate. Only grain boundaries in polycrystalline ZnO may provoke p-type conducting films [16] under oxygen-rich conditions. In general the addition of oxygen is thought to reduce the number of oxygen vacancies which are supposed to be the key donor defects. We believe that an understanding of the effect of oxygen addition has to be extended to take the grain boundaries into account. Under oxygen-rich conditions the percentage of grain boundaries with undercoordinated oxygen atoms increases. In previous work [12,18] we have shown that such grain boundaries contribute shallow levels above the VB edge. These are equivalent to the defect levels of v_{Zn} in bulklike ZnO or ZMO discussed here since the oxygen atoms at the grain boundaries are undercoordinated due to local Zn deficiencies. Furthermore, nitrogen at grain boundaries can form shallow defect levels which are very similar to those shown in Fig. 5 (see Fig. 11 in Ref. [12]). We argue therefore that all these shallow levels are activated due to the depletion zones near grain boundaries [16,52]. Zhang *et al.* interpret their experimental results along this line [9], and Wang et al. even suppose that oxygen excess causes the formation of a quasi-two-dimensional hole gas, which could explain the very high mobilities seen in some experiments (see Ref. [16] and references therein).

Putting all of this together, this rather general defect-complex mechanism for promoting p-type conductivity in ZnO, ZMO, and related materials emerges: defect complexes which are connected to the zinc vacancies in the bulk interior or at grain boundaries provide shallow defect levels which can serve as acceptor defects. The activation of these defects by lowering the net electron concentration is provided either by codoping (e.g., N and Mg [17]) or by depletion zones around grain boundaries.

IV. SUMMARY

We have studied the electronic densities of states of crystalline ZnO and $Zn_{1-x}Mg_xO$ with $0 \leqslant x \leqslant 0.4$. We have shown that the SIC-LDA allows us to calculate the electronic band gap as a function of the Mg content and leads to quantitatively reasonable results with respect to experimental data.

We have determined the electronic defect levels which are generated by the introduction of N_O substitutional defects. They are at 0.25 eV above the VB or higher. An increasing number of neighboring Mg atoms to the N_O site shifts the defect level even deeper into the band gap. On the other hand, isolated v_{Zn} defects generate shallow levels attached to the VB edge. In combination with N_O, the defect complex N_O-v_{Zn} produces low-lying defect levels which emerge continuously above the VB, and no detached gap states (like in the case of the isolated N_O defect) appear. It is likely that these levels which are peaked at 125–140 meV are connected to experimentally determined acceptor levels which are reported at 130 meV [13], 160 meV [24], or 190 meV [49]. Neighboring Mg atoms of the N_O-v_{Zn} defect complex do not change the situation significantly. Apparently, the role of Mg is mainly a lowering of the net electron concentration which lowers the Fermi level and therefore contributes the N_O-v_{Zn} defect complexes as acceptors.

Our presented results are consistent with those of an earlier study on ZnO grain boundaries [12,18], in which we found that at grain boundaries with local Zn deficiencies (which is equivalent to undercoordinated oxygen atoms), N_O defects at

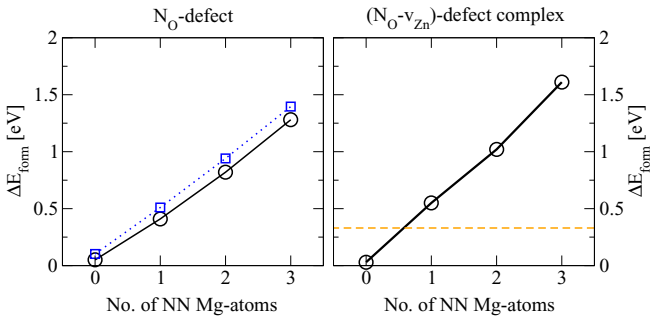

FIG. 8. Increase of the defect formation energy of the N_O defect (left) and the N_O-v_{Zn} complex (right) with increasing number of next-neighbor Mg atoms. The energy differences ΔE_{form} are calculated with respect to the values obtained for bulk ZnO. Results from Ref. [48] are shown as a dotted line for comparison in the left panel. The sum of the formation energies of isolated N_O and v_{Zn} (without next-neighbor Mg atoms) is shown as a dashed line in the right panel.

the grain boundary produce shallow defect levels without gap to the VB edge and are thus promising acceptor levels.

The following conclusion emerges from this work: one condition for *p*-type conductivity in ZnO, ZMO, or related materials is to have enough *p*-type defects like, for example, N_O which interact with v_{Zn} point defects or local Zn deficiencies in extended defects like grain boundaries in order to form shallow gapless defect levels above the VB edge. Moreover, the net electron concentration has to be low enough to make these shallow acceptor states partially unoccupied. This second condition can be achieved by Mg_{Zn}/N_O codoping in the bulk interior or by N_O doping at grain boundaries to create depletion zones.

ACKNOWLEDGMENTS

Financial support for this work was provided by the European Commission through Contract No. NMP3-LA-2010-246334 (ORAMA).

APPENDIX

1. Defect formation energies

The defect formation energies of the zinc vacancy and the N_O substitutional defect in ZnO have recently been discussed in great detail (see, e.g., Refs. [12,15,34,53–56] and references therein). For a discussion of defect formation energies in ZnO obtained from SIC-LDA we refer the reader to Refs. [18,34]. Here we want to focus on the effect of the Mg atoms on the defect formation energies E_{form} of N_O and the N_O-v_{Zn} complex.

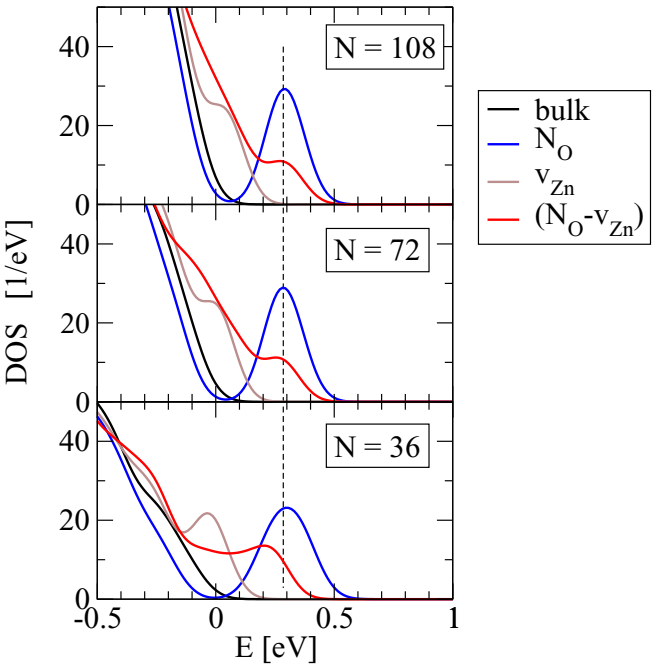

FIG. 9. Zoom of the DOS in the vicinity of the valence-band edge, showing the defect levels of N_O, v_{Zn}, and the N_O-v_{Zn} complex calculated for three different supercell sizes.

E_{form} is found to depend strongly on the number of Mg atoms that are nearest neighbors to the defect site, which can be explained by a stronger Zn-N bond compared to the Mg-N bond. Figure 8 shows the increase in E_{form} with respect to bulk ZnO with an increasing number of next-nearest-neighbor Mg atoms. Our results are in line with the findings of Gai *et al.* [48], who have performed DFT simulations using cubic zinc-blende ZMO alloys. Note that the formation of a N_O-v_{Zn} complex is energetically favorable by 0.3 eV compared to a pair of isolated N_O and v_{Zn} point defects without Mg atoms in the direct vicinity of the N atom.

2. Supercell size effects

In order to check the influence of the finite supercell size on the defect levels obtained from our DOS calculations, we have compared calculations for three different supercell sizes, namely, $N = 36$, 72, and 108 atoms. As shown in Fig. 9, there is very little change in level position and peak shape when comparing the results for 72- and 108-atom supercells. On the other hand, the 36-atom supercells do not yet yield fully converged results, although the general conclusions could qualitatively also be drawn from these rather small cells. We therefore decided to use the 72-atom supercells for the results presented in the main text.

[1] E.-C. Lee, Y.-S. Kim, Y.-G. Jin, and K. J. Chang, Phys. Rev. B **64**, 085120 (2001).

[2] E.-C. Lee and K. J. Chang, Phys. Rev. B **70**, 115210 (2004).

[3] W.-J. Lee, J. Kang, and K. J. Chang, Phys. Rev. B **73**, 024117 (2006).

[4] C. H. Park, S. B. Zhang, and S. H. Wei, Phys. Rev. B **66**, 073202 (2002).

[5] S. Limpijumnong, S. B. Zhang, S.-H. Wei, and C. H. Park, Phys. Rev. Lett. **92**, 155504 (2004).
[6] Y. Yan and S.-H. Wei, Phys. Status Solidi **245**, 641 (2008).
[7] L. G. Wang and A. Zunger, Phys. Rev. Lett. **90**, 256401 (2003).
[8] Y. Yan, J. Li, S. H. Wei, and M. M. Al-Jassim, Phys. Rev. Lett. **98**, 135506 (2007).
[9] C. Y. Zhang, X. M. Li, X. D. Gao, J. L. Zhao, K. S. and J. M. Bian, Chem. Phys. Lett. **420**, 448 (2006).
[10] J. L. Lyons, A. Janotti, and C. G. Van de Walle, Appl. Phys. Lett. **95**, 252105 (2009).
[11] S. Lany and A. Zunger, Phys. Rev. B **81**, 205209 (2010).
[12] W. Körner and C. Elsässer, Phys. Rev. B **81**, 085324 (2010).
[13] J. G. Reynolds, C. L. Reynolds, Jr., A. Mohanta, J. F. Muth, J. E. Rowe, H. O. Everitt, and D. E. Aspnes, Appl. Phys. Lett. **102**, 152114 (2013).
[14] L. Liu, J. Xu, D. Wang, M. Jiang, S. Wang, B. Li, Z. Zhang, D. Zhao, C.-X. Shan, B. Yao, and D. Z. Shen, Phys. Rev. Lett. **108**, 215501 (2012).
[15] M. N. Amini, R. Saniz, D. Lamoen, and B. Partoens, Phys. Chem. Chem. Phys. **17**, 5485 (2015).
[16] B. Wang, J. Min, Y. Zhao, W. Sang, and C. Wang, Appl. Phys. Lett. **94**, 192101 (2009).
[17] A. Hierro, G. Tabares, J. M. Ulloa, E. Muñoz, A. Nakamura, T. Hayashi, and J. Temmyo, Appl. Phys. Lett. **94**, 232101 (2009).
[18] W. Körner and C. Elsässer, Phys. Rev. B **83**, 205315 (2011).
[19] W. Körner, D. F. Urban, D. M. Ramo, P. D. Bristowe, and C. Elsässer, Phys. Rev. B **90**, 195142 (2014).
[20] S. Sallis, K. T. Butler, N. F. Quackenbush, D. S. Williams, M. Junda, D. A. Fischer, J. C. Woicik, N. J. Podraza, B. E. White, Jr., A. Walsh, and L. F. J. Piper, Appl. Phys. Lett. **104**, 232108 (2014).
[21] S. Sallis, N. F. Quackenbush, D. S. Williams, M. Senger, J. C. Woicik, B. E. White, and L. F. J. Piper, Phys. Status Solidi A **212**, 1471 (2015).
[22] W. Körner, D. F. Urban, and C. Elsässer, J. Appl. Phys. **114**, 163704 (2013).
[23] W. Körner, D. F. Urban, and C. Elsässer, Phys. Status Solidi A **212**, 1476 (2015).
[24] A. Kurtz, A. Hierro, E. Muñoz, S. K. Mohanta, A. Nakamura, and J. Temmyo, Appl. Phys. Lett. **104**, 081105 (2014).
[25] P. E. Blöchl, Phys. Rev. B **50**, 17953 (1994).
[26] G. Kresse and J. Furthmüller, Phys. Rev. B **54**, 11169 (1996).
[27] G. Kresse and D. Joubert, Phys. Rev. B **59**, 1758 (1999).
[28] J. H. Rose, J. Ferrante, and J. R. Smith, Phys. Rev. Lett. **47**, 675 (1981).
[29] C. Elsässer, N. Takeuchi, K. M. Ho, C. T. Chan P. Braun, and M. Fähnle, J. Phys. Condens. Matter **2**, 4371 (1990).
[30] K. M. Ho, C. Elsässer, C. T. Chan, and M. Fähnle, J. Phys. Condens. Matter **4**, 5189 (1992).
[31] B. Meyer, K. Hummler, C. Elsässer, and M. Fähnle, J. Phys. Condens. Matter **7**, 9201 (1995).
[32] F. Lechermann, M. Fähnle, B. Meyer, and C. Elsässer, Phys. Rev. B **69**, 165116 (2004).
[33] W. Körner, P. D. Bristowe, and C. Elsässer, Phys. Rev. B **84**, 045305 (2011).
[34] W. Körner and C. Elsässer, Phys. Rev. B **83**, 205306 (2011).
[35] J. P. Perdew and A. Zunger, Phys. Rev. B **23**, 5048 (1981).
[36] D. Vanderbilt, Phys. Rev. B **32**, 8412 (1985).
[37] D. Vogel, P. Krüger, and J. Pollmann, Phys. Rev. B **54**, 5495 (1996).
[38] H. Ryoken, N. Ohashi, I. Sakaguchi, Y. Adachi, S. Hishita, and H. Haneda, J. Cryst. Growth **287**, 134 (2006).
[39] R. Ghosh and D. Basak, J. Appl. Phys. **101**, 023507 (2007).
[40] A. Kaushal and D. Kaur, Sol. Energy Mater. Sol. Cells **93**, 193 (2009).
[41] H. Nishinaka, Y. Kamada, N. Kameyama, and S. Fujita, Phys. Status Solidi B **247**, 1460 (2010).
[42] B. Laumer, F. Schuster, M. Stutzmann, A. Bergmaier, G. Dollinger, and M. Eickhoff, J. Appl. Phys. **113**, 233512 (2013).
[43] C. Franz, M. Giar, M. Heinemann, M. Czerner, and C. Heiliger, MRS Proc. **1494**, 57 (2013).
[44] E. Gür, G. Tabares, A. Arehart, J. M. Chauveau, A. Hierro, and S. A. Ringel, J. Appl. Phys. **112**, 123709 (2012).
[45] C. W. Teng, J. F. Muth, U. Ozgur, M. J. Bergmann, H. O. Everitt, A. K. Sharma, C. Jin, and J. Narayan, Appl. Phys. Lett. **76**, 979 (2000).
[46] W. I. Park, G.-C. Yi, and H. M. Yang, Appl. Phys. Lett. **79**, 2022 (2001).
[47] *Semiconductors: Physics of Group 4 Elements and 3-5 Compounds*, edited by K. H. Hellwege and O. Madelung, Landbolt-Börnstein, New Series, Group 3, Vol. 17, Pt. A (Springer, Berlin, 1982); *Semiconductors: Intrinsic Properties of Group 4 Elements and 3-5-7 and 1-7 Compounds*, edited by O. Madelung, W. von der Osten, and U. Rössler, Landolt-Börnstein, New Series, Group 3, Vol. 22, Pt. A (Springer, Berlin, 1987).
[48] Y. Q. Gai, B. Yao, Z. P. Wei, Y. F. Li, Y. M. Lu, D. Z. Shen, J. Y. Zhang, D. X. Zhao, X. W. Fan, J. Li, and J.-B. Xia, Appl. Phys. Lett. **92**, 062110 (2008).
[49] P. Muret, D. Tainoff, C. Morhain, and J. M. Cauveau, Appl. Phys. Lett. **101**, 122104 (2012).
[50] Y. F. Li, B. Yao, Y. M. Lu, Z. P. Wei, Y. Q. Gai, C. J. Zheng, Z. Z. Zhang, B. H. Li, D. Z. Shen, X. W. Fan, and Z. K. Tang, Appl. Phys. Lett. **91**, 232115 (2007).
[51] M. X. Qiu, Z. Z. Ye, H. P. He, Y. Z. Zhang, X. Q. Gu, L. P. Zhu, and B. H. Zhao, Appl. Phys. Lett. **90**, 182116 (2007).
[52] M. A. Alim, S. Li, F. Liu, and P. Cheng, Phys. Status Solidi A **203**, 410 (2006).
[53] S. J. Clark, J. Robertson, S. Lany, and A. Zunger, Phys. Rev. B **81**, 115311 (2010).
[54] A. Janotti and C. G. Van de Walle, Phys. Rev. B **76**, 165202 (2007).
[55] F. Oba, A. Togo, I. Tanaka, J. Paier, and G. Kresse, Phys. Rev. B **77**, 245202 (2008).
[56] S. Sakong, J. Gutjahr, and P. Kratzer, J. Chem. Phys. **138**, 234702 (2013).